ELSEVIER

Journal of Alloys and Compounds 317–318 (2001) 372–378

Journal of ALLOYS AND COMPOUNDS

www.elsevier.com/locate/jallcom

The effect of microstructure on hardness measurements in the aluminium-rich corner of the Al–Ni–Cr system

D.N. Compton[a,*], L.A. Cornish[a], M.J. Witcomb[b]

[a]*School of Process and Materials Engineering, University of the Witwatersrand, Private Bag 3, Johannesburg, WITS 2050, South Africa*
[b]*Electron Microscope Unit, University of the Witwatersrand, Private Bag 3, Johannesburg, WITS 2050, South Africa*

Abstract

Arc-melted Al-rich samples from the Al–Cr–Ni system were analysed using optical microscopy, scanning electron microscopy, energy dispersive X-ray spectroscopy and X-ray diffraction. All of the expected binary phases were observed and identified. The binary phase with the largest extension into the ternary was Al_3Ni_2 at about 12 at.%. Three separate ternary phases were identified from the microstructures, and were found to agree reasonably with the compositions in the literature, although the phase fields had different shapes. Vicker's microhardness measurements have indicated that the phase hardnesses in decreasing order are most likely: Al_3Ni_2, ϕ, (αCr), ρ, Al_4Cr, Al_7Cr, $Al_{11}Cr_2$, Al_9Cr_4, Al_3Ni and (Al). The ϕ, Al_4Cr, $Al_{11}Cr_2$ and Al_3Ni phases were brittle in massive form.

Keywords: Hardness measurements; Al–Cr–Ni phase diagram

1. Introduction

Al–Cr–Ni alloys are important as the basis of the γ/γ′ microstructure, excellent high temperature oxidation and mechanical properties of superalloys. Overlay coatings have been used increasingly, and their effectiveness originates from the combined ability of Al and Cr within the coatings to form a self-healing and protective layer of alumina and chromia [1,2]. Higher Al content alloys are also of interest, not only because of the oxide-forming ability of aluminium, but also because βAlNi/(αCr) systems have shown potential for good mechanical properties, as well as weight reduction through the lower density phases [3–5].

Although the binary systems are generally well-understood [6], until recently there has been little data on high-aluminium content alloys in the Al–Cr–Ni system. The current study was initiated as part of a more extensive characterisation of the Al–Cr–Ni–Ru system. Alloys were studied in the as-cast condition in order to derive the liquidus surface, and also the likely phase extents on solidification.

2. Previous work

2.1. Al–Cr–Ni phase diagram

The binary systems are well-known, and largely agree with the compilation by Massalski [6]. In common with usual terminology: γ is the solid solution based on nickel, γ′ the phase based on $AlNi_3$, βAlNi the compound based on AlNi, and (αCr) is the solid solution based on chromium. Although much literature has been published describing the Al–Cr–Ni system, only work which is pertinent to the high Al-content region of the phase diagram is discussed here.

Merchant and Notis [7] reviewed available data and gave a critical evaluation. They reported that Kornilov and Mints [8], using hardness and resistivity measurements, indicated a quasi-binary eutectic in the AlNi–Cr isopleth between (αCr) and βAlNi at 1445°C and a liquid composition of 33.2 at.% Al, 33.6 at.% Cr and 33.2 at.% Ni, and with both solid phases showing limited regions of solid solubility.

Merchant and Notis [7] reported Tu's [9] ternary τ phase, noting that it was the first time such a phase had been described, at approximately 75 at.% Al, 15 at.% Cr and 10 at.% Ni. No match could be found with existing phases using X-ray diffraction [7].

*Corresponding author.

0925-8388/01/$ – see front matter
PII: S0925-8388(00)01441-9

Audier et al. [10] studied the Al–Cr system up to 40 at.% Cr using transmission electron microscopy (TEM) to study the structures, after experiencing difficulties in interpreting the structures in ternary alloys [11], and resolved some of the phases. Rosell-Laclau et al. [11] studied the Al-rich corner of the Al–Cr–Ni system, especially near the binaries. They identified the solidification sequence mainly by the microstructures, as well as the phase sequence in the quenched DTA samples. The morphology of βAlNi was non-facetted regardless of the cooling rate, whereas that of Al_3Ni_2 was more facetted and accicular with higher cooling rates. Three ternary compounds were found [11]. The variation of chromium in the (Al), Al_3Ni, Al_3Ni_2 phases, and nickel in (Cr), γAl_9Cr_4, ξAl_8Cr_5 phases were minimal and was not dependent on the cooling rate. The βAlNi and ϕ phases showed a much wider range of solid solubility, whereas the ternary λ and ρ phases exhibited much smaller ranges. Little contrast in backscattered electron imaging was observed between the ϕ, λ and θAl_7Cr phases and similarly, between the ρ and $Al_{11}Cr_2$ phases.

The ternary phase structures were complex [11]; not only were some of the individual structures related to each other, for example, via the polyhedra, but also there were polytypes within the structures, as well as an ordering effect. The θ ternary phase was directly related to the binary monoclinic θAl_7Cr phase, and the η phase was identical to orthorhombic $\eta Al_{11}Cr_2$. The ϕ ternary phase was revealed to be monoclinic, and there was also an orthorhombic polytype. The λ ternary phase was orthorhombic. Finally, the ρ ternary phase exhibited an intergrowth of metastable rhombohedral and hexagonal structures with indistinguishable compositions. There was also a stable third variant, which is hexagonal.

Rosell-Laclau et al. [11] showed a liquidus surface which was dominated initially by the (αCr)–βAlNi eutectic, agreeing with previous workers [7,8], which was subsequently replaced by other reactions; in other words, the Al-rich corner resembled a symmetrical leaf, albeit with the ternary surfaces spoiling that symmetry.

Huang and Chang [12] reviewed current data and employed thermodynamic modelling to produce the full Al–Cr–Ni phase diagram. They used simplified phase descriptions [14] compared with Dupin [13,15], and fewer ternary interaction parameters. Their [12] liquidus surface in the Al corner was more irregular than that of Rosell-Laclau et al. [11], and the surfaces of primary solidification were produced for the following phases: (γNi), $\gamma'AlNi_3$, βAlNi, (αCr), Al_8Cr_5_H, Al_9Cr_4_H, Al_8Cr_5_L, Al_9Cr_4_L, Al_4Cr, $Al_{11}Cr_2$, $Al_{13}Cr_2$, (Al), Al_3Ni and Al_3Ni_2. Interestingly, the Al_8Cr_5_L phase exhibited a liquidus surface which did not touch the binary; it was behaving as a ternary phase.

2.2. Mechanical properties

Much rigorous work has been carried out on βAlNi compounds of different stoichiometries, in single and polycrystal forms, and with various alloying additions, which has been reviewed by Vedula and Khadkikar [16], Noebe et al. [17], and Baker and Munroe [18]. The most deleterious property is the inherent brittleness, and thus much work has been done to improve the ductility. Stoichiometry is very important since structures with increasing non-stoichiometry have more point defects. Moving away from stoichiometry there is an increase of yield stress, since the mobile $a\langle 100\rangle\{001\}$ dislocations become difficult to move when they encounter point defects [19], such as vacancies and antistructure atoms [16–18]. Westbrook [20] showed that the hardness increase away from stoichiometry was much greater on the Al-rich side. Additionally, interfaces can act as both dislocation sources encouraging ductility, or barriers which cause dislocation pile-up, and hence cracking. Evidence shows that fine-grained structures are more ductile, since there are fewer dislocations per unit area of interface [17].

When Cr was added to βAlNi, the slip vector was changed, but there was no improvement in ductility [21,22]. With higher Cr content, Frommeyer and Derder [23] chose AlNi–(αCr) alloys to benefit from the eutectic microstructure in their study of deformation behaviour, the alloys containing up to 28 at.% Cr. They found that large amounts of deformation broke up the as-cast lamellar microstructure. Using TEM, they observed misfit dislocations at the interfaces, and found that the emission of mobile $a\langle 100\rangle\{001\}$ dislocations from either phase increased the ductility. They [23] showed that the plastic strain was a maximum at 27 at.% Cr, which represented the optimal (αCr) particle separation in the AlNi matrix, as well as the mobility of the interphase dislocations. Two-phase structures exhibited better fracture toughness than single phase alloys, due to the dislocation mobility.

3. Experimental procedure

The purity of the elements was at least 99.9 wt.%. The alloy charges were weighed, mixed and then arc-melted. There was no attempt made to compact the raw materials since powders were not used. Arc-melting was carried out under an argon atmosphere with a titanium oxygen-getter, and the samples were inverted and remelted to ensure thorough mixing. Loss of aluminium was found to be minimal.

The sample buttons were cut in half as accurately as possible (in order to observe the entire cross-sectional structure), using a diamond wheel. Sections were prepared metallographically and examined by optical microscopy and SEM (Jeol JSM-840), using the secondary and backscattered electron imaging modes. Analyses were undertaken using energy dispersive spectroscopy (Link AN10000 system), with elemental standards, and at least five analyses were taken per phase. Overall analyses were

also taken. EDS analyses were consistent, within 1 at.% in most cases.

X-ray diffraction was conducted on bulk samples using a Philips PW1820 diffractometer with copper radiation. Since there was a lack of data for some of the phases, the known lattice parameters and space groups from literature were input to the 'CC Miller' program to obtain the angles and intensities over a specified range to calculate the *d*-spacings [24], and also input to 'Crystallographica' [25]. The input conditions were set to be as close to the experimental conditions as possible.

Vicker's microhardness measurements were undertaken on a Shimadzu Microhardness Tester, Type M, using a load of 1000 g for 10 s. At least five measurements were made on representative multiphase regions of each sample, and any cracks were noted. At this stage, no attempt was made to measure the microhardness of the individual phases, because very few of them were deemed large enough.

4. Results

4.1. Al–Cr–Ni phase diagram

The phases were mainly identified by studying the microstructures, EDS and X-ray diffraction analyses, and these results are reported elsewhere [26], although the results are used as a basis for the hardness plots here. Although the nomenclature of Rosell-Laclau et al. [11] was used, the phases were identified from their solidification sequence, rather than employing more rigorous TEM and modelling techniques. Some of the microstructures are shown in Figs. 1–4.

4.2. Hardness measurements

The Vicker's microhardness measurements ranged from

Fig. 1. SEM image in backscattered electron mode: Nominal Al_{64}:Cr_{21}:Ni_{15} (ANC019) showing Al_9Cr_4 dendrites (medium grey), ϕ peritectic layer (dark grey), with Al_9Cr_4+Al_3Ni_2 (light) eutectic. Bar represents 10 μm.

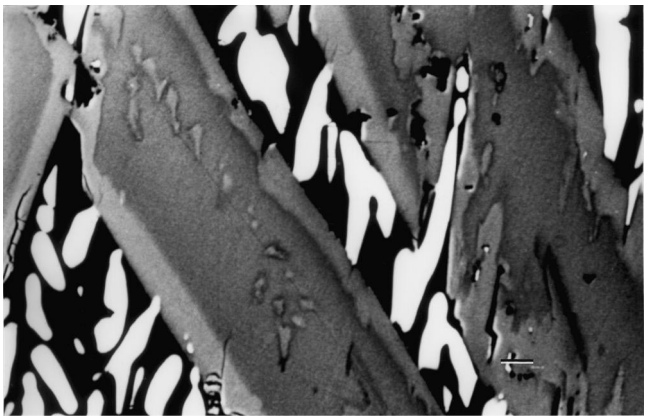

Fig. 2. SEM image in backscattered electron mode: Nominal Al_{79}:Cr_{10}:Ni_{11} (ANC001) showing ϕ plates (dark grey), peritectic λ (light grey) at the plate edges, with Al_3Ni dendrites (light) and indiscernible Al_3Ni+(Al) (dark) eutectic between the plates. Bar represents 10 μm.

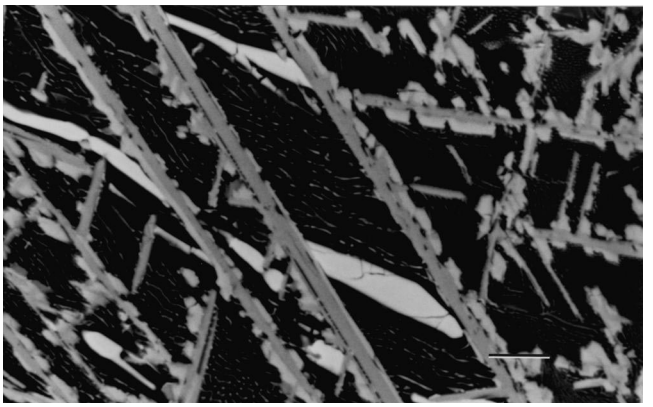

Fig. 3. SEM image in backscattered electron mode: Nominal Al_{90}:Cr_5:Ni_5 (ANC017) showing $Al_{11}Cr_2$ plates (dark grey), Al_7Cr peritectic layer (light grey), and Al_3Ni needles (light) in Al_3Ni+(Al) eutectic between the plates. Bar represents 10 μm.

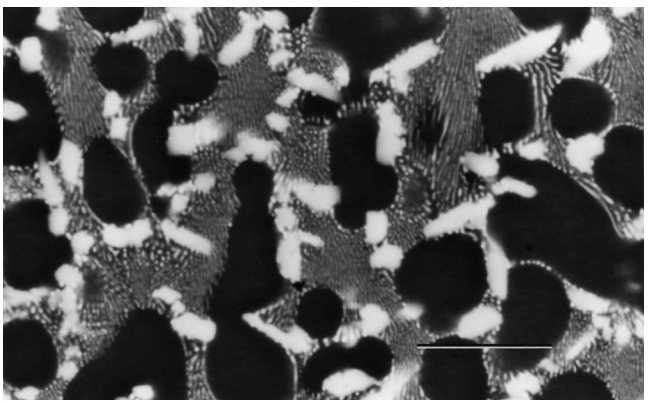

Fig. 4. SEM image in backscattered electron mode: Nominal Al_{96}:Cr_2:Ni_2 (ANC015) showing Al_7Cr (light), (Al) (dark), and Al_3Ni (light grey)+(Al) eutectic. Bar represents 10 μm.

~800 HV_1 to ~50 HV_1 in the Al-rich corner, and are shown in Table 1 and plotted with the phase compositions in Fig. 5 (without tie-lines for clarity). The only hardness obtained on an individual phase was the primary ϕ in Al_{79}:Cr_{10}:Ni_{11} (ANC001): 297±HV_1. Some of the alloys had wide variations, which is due to the varying proportions of the phases in the microstructures. There could also have been an effect from porosity, although regions with visible porosity were avoided. Cracks were observed in most of the alloys, and were present in various forms: edge and corner cracks, but the edge cracks were not recorded in the table. One alloy, Al_{85}:Cr_{12}:Ni_3 (ANC014) had such a wide variation in behaviour that no values were tabulated, although the maximum hardness was 290 HV_1.

Alloys comprising only βAlNi and (αCr) were more ductile than the others, as demonstrated by the bowed edges of the hardness indentations. The Al_{43}:Cr_{52}:Ni_5 (ANC012) alloy comprising mainly (αCr) also showed substantial deformation, without cracking. Unsurprisingly, all of the very high Al-content alloys were also very ductile. Often the cracks were observed mainly in the primary phase, and did not propagate into the eutectic. Thus, the brittle nature of the primary ϕ, Al_3Ni, Al_4Cr and $Al_{11}Cr_2$ phases was revealed.

There is a peak in the hardness values around 800 HV_1 for alloys comprising Al_3Ni_2 and ϕ. An alloy with a high proportion of (αCr), Al_{43}:Cr_{52}:Ni_5 (ANC012), also gave a high value (~760 HV_1). Combinations of the ρ with the high Al-content intermetallic phases (Al_4Cr, Al_3Ni, $Al_{11}Cr_2$ and Al_9Cr_4) gave hardnesses between 500 and 600 HV_1. Near the Al-rich corner, the hardness values decreased rapidly. A combination of the ϕ, Al_3Ni and (Al) phases gave a value of approximately 315 HV_1, whereas the more Al-rich combination of $Al_{11}Cr_2$, Al_3Ni and (Al), even with Al_7Cr, gave values around 150 HV_1. The presence of some $Al_{11}Cr_2$ in the Al_3Ni+(Al) eutectic increased the hardness to 70 HV_1, compared with the purely eutectic Al_3Ni+(Al) alloys which had values around 50 HV_1.

5. Discussion

The phases identified were: βAlNi, Al_3Ni_2, Al_3Ni, (Al), (αCr), Al_8Cr_5, Al_9Cr_4, Al_4Cr, $Al_{11}Cr_2$ and Al_7Cr, together with the ternary phases: ϕ, ρ and λ. All of the expected binary phases [6] were observed and identified. Three separate ternary phases were identified from the microstructures and analyses, and were found to agree reasonably with the compositions of Tu [9] and Rosell-Laclau et

Table 1
Microhardness values of the alloys

Sample	Composition	HV		Major phases
ANC001	Al_{79}:Cr_{10}:Ni_{11}	311±12	D[a]	ϕ, λ, Al_3Ni, (Al)
ANC003	Al_{58}:Cr_{33}:Ni_9	808±30	C[a]	Al_8Cr_5, Al_3Ni_2
ANC004	Al_{36}:Cr_{11}:Ni_{53}	492±6	D	AlNi, (Cr)
ANC005	Al_{35}:Cr_{33}:Ni_{32}	568±26	D	AlNi, (Cr)
ANC007	Al_{78}:Cr_{19}:Ni_3	573±26	C	Al_4Cr, Al_3Ni, (Al),
ANC008	Al_{69}:Cr_6:Ni_{25}	763±36	C	ϕ, Al_3Ni, Al_3Ni_2
ANC009	Al_{67}:Cr_{21}:Ni_{12}	781±12	C	ϕ, Al_9Cr_4, Al_3Ni_2
ANC010	Al_{55}:Cr_{19}:Ni_{26}	830±10	C	Al_3Ni_2, Al_8Cr_5
ANC011	Al_{49}:Cr_{35}:Ni_{16}	809±9	C	Al_8Cr_5, Al_3Ni_2, (Cr)
ANC012	Al_{43}:Cr_{52}:Ni_5	760±7	D	Al_8Cr_5, Al_3Ni_2, (Cr)
ANC013	Al_{71}:Cr_{25}:Ni_4	717±30	C	ϕ, ρ, Al_9Cr_4
ANC014	Al_{85}:Cr_{12}:Ni_3	Data erratic		Al_4Cr, $Al_{11}Cr_2$, Al_7Cr, Al_3Ni, (Al)
ANC015	Al_{96}:Cr_2:Ni_2	70±3	D	Al_7Cr, Al_3Ni, (Al)
ANC016	Al_{93}:Cr_5:Ni_2	140±7	D	$Al_{11}Cr_2$, Al_3Ni, (Al), Al_7Cr
ANC017	Al_{90}:Cr_5:Ni_5	143±10	D	$Al_{11}Cr_2$, Al_3Ni, (Al)
ANC018	Al_{88}:Cr_2:Ni_{10}	153±16		Al_3Ni, Al_7Cr, (Al)
ANC019	Al_{64}:Cr_{21}:Ni_{15}	795±22	C	ϕ, Al_9Cr_4, Al_3Ni_2
ANC020	Al_{48}:Cr_{17}:Ni_{35}	785±32		AlNi
ANC021	Al_{90}:Cr_9:Ni_1	154±11		Al_4Cr, Al_7Cr, Al_3Ni, (Al)
ANC022	Al_{86}:Cr_9:Ni_5	203±14		$Al_{11}Cr_2$, Al_3Ni, (Al)
ANC023	Al_{79}:Cr_{10}:Ni_{11}	328±39	C	ϕ, Al_3Ni, (Al)
ANC024	Al_{94}:Cr_4:Ni_2	101±10	D	$Al_{11}Cr_2$, Al_3Ni, (Al)
ANC025	Al_{90}:Cr_4:Ni_6	151±7	D	$Al_{11}Cr_2$, Al_3Ni, (Al)
ANC026	Al_{98}:Ni_2	48±1	D	Al_3Ni, (Al)
ANC027	Al_{71}:Cr_{21}:Ni_8	686±28	C	ρ, λ, Al_9Cr_4, Al_3Ni
ANC028	Al_{77}:Cr_{21}:Ni_2	565±53	C	ρ, Al_9Cr_4, Al_4Cr
ANC029	Al_{76}:Cr_{15}:Ni_9	417±51	C	ρ, Al_3Ni, (Al)
ANC030	Al_{80}:Cr_{18}:Ni_2	515±25	C	Al_4Cr, $Al_{11}Cr_2$
ANC031	Al_{71}:Cr_{27}:Ni_2	617±38	C	ρ, Al_9Cr_4, Al_8Cr_5
ANC032	Al_{67}:Cr_{23}:Ni_{10}	730±23	C	Al_9Cr_4, Al_3Ni_2, ϕ, ρ

[a] C indicates cracking; D indicates deformation.

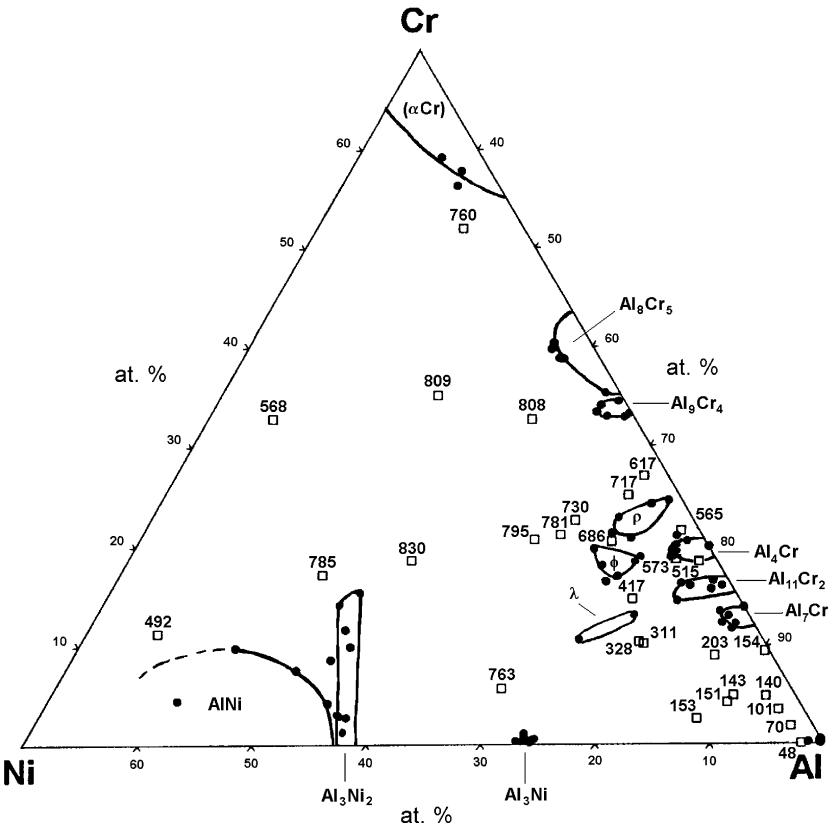

Fig. 5. Microhardness values plotted on the projection of the solid phases. The solid circles represent the composition of the phases found in the alloys. The tie-lines have been removed for clarity.

al. [11], although the phase fields had different shapes, especially that of ρ, which was much larger than reported [11]. However, the agreement in both analyses and morphology was such that the nomenclature of Rosell-Laclau et al. [11] was used.

The shape of the liquidus surface was rather different from that of Rosell-Laclau et al. [11], although the phases were the same. There was much better agreement in shape with the calculated liquidus projection of Huang and Chang [12]. However, they did not present any ternary phases, although there were high and low temperature forms of both Al_8Cr_5 and Al_9Cr_4. The current work shows that both the liquidus surfaces of Al_3Ni_2 and Al_3Ni are much larger than previously calculated.

Physical properties, including hardness, depend on the actual phases present, as well as their proportions and distributions. No data on the hardness of the ternary alloys have been found in the literature, although Westbrook has reported ~320 $kg \cdot mm^{-2}$ for binary βAlNi [20], and Cornish et al. [27] gave 277±11 HV. The alloy with the highest proportion of βAlNi in this investigation was Al_{36}:Cr_{11}:Ni_{53} (ANC004), which comprised mainly cored βAlNi and a little βAlNi+(αCr) eutectic and its hardness was 492 HV_1. The difference between these values suggests both the hardening effect of the interdendritic βAlNi+(αCr) eutectic, as well as the solid solution strengthening effect of Cr. For the Al–Ni–Ru system, where Ru substitutes Ni in βAlNi, Wolff and Sauthoff [28] gave values of ~400±35 HV at $x_{Ru}=0$, to ~800±30 HV for $x_{Ru}\approx0.25$, whereas Cornish et al. [27] had: ~277±11 HV at $x_{Ru}=0$, and ~529±33 HV for $x_{Ru}\approx0.27$ from as-cast samples. In this work, the effect of Cr substitution in βAlNi had a greater effect on hardness than a similar amount of Ru [28,29].

The highest hardnesses in this investigation were from the combination of the Al_3Ni_2 and φ phases (~800 HV_1), with Al_3Ni_2 being the hardest phase, followed by alloys with a high (αCr) content (~760 HV_1). Thus, these phases are expected to be the hardest, and although they might also be expected to be brittle, only the φ phase showed substantial cracks. Intermediate hardnesses were revealed for ρ, Al_4Cr, Al_3Ni, $Al_{11}Cr_2$ and Al_9Cr_4 phases, since combinations of these intermetallic phases gave hardnesses between 500 and 600 HV_1. The Al_4Cr, Al_3Ni and $Al_{11}Cr_2$ phases were also shown to be brittle in massive form by exhibiting cracks. The φ phase probably has a hardness in the region of 500 HV_1 (despite the measured values), since with the much softer Al_3Ni and (Al) matrix, it still gave a value of approximately 315 HV_1. Comparing the hardness of the multiphase alloys, the next hardest phase in this decreasing scale is likely to be Al_7Cr (~150 HV_1), then $Al_{11}Cr_2$ (~70 HV_1), followed by Al_3Ni (~50 HV_1), and

finally (Al). The hardness of the latter was not measured, although Horner [29] gave a value of ~70 HV_1.

The phase morphology obviously has an effect, and phases usually have different morphologies when forming first, than when they form subsequently. The high hardness and ductility of ANC019 (Fig. 1) is due to the specific phases, as well as the eutectic morphology. The composite-like combination of plates in Fig. 2 (ANC001) also gave good properties. The Al_3Ni phase was shown to be brittle in massive primary form, but when present as a discrete phase in the eutectic, exhibited ductile behaviour. Samples with this eutectic (Figs. 3 and 4) were noticeably softer. In order to study the effect of morphology systematically, the samples would need to be heat treated in order to provide more control of the morphology. Solid state precipitation, observed in the βAlNi, Al_3Ni_2 and Al_8Cr_5 phases, would also have increased the hardnesses, because the matrix would have had additional strain around the particles.

The plot of the hardness values of the alloys on the projection of the liquidus surface can show whether the primary phase is a major influence on the hardness. Of course, the proportions of the primary phase will vary across the primary surface of solidification, but the plot can still be used as a guide. Fig. 6 shows that there is a systematic trend within the Al_9Cr_2 primary solidification surface: hardness decreases as alloys become less Ni-rich and more Al-rich. Hardnesses of alloys with primary (αCr) increase as the composition nears the primary solidification surface of Al_3Ni_2, arguably the hardest phase in this investigation. Where the alloys within a primary surface of solidification also have many other phases forming subsequently, the plot is less helpful, but a trend can still be observed. Additionally, the hardness of alloys within the Al_4Cr and $Al_{11}Cr_2$ surfaces decrease as the compositions become increasingly Al-rich.

Although the hardness measurements described can be used as a guide to the mechanical properties of these alloys and their constituent phases, they do not indicate the effects of stoichiometry, nor defects. In order to take account of these factors, single-phase materials are preferred.

6. Conclusions

This investigation of as-cast arc-melted buttons indicated the presence of all the expected binary phases, although Al_3Ni and (Al) showed very limited solubility within the ternary. Additionally, the ternary phases: ϕ, ρ and λ were identified. The surfaces of primary solidification were similar to those in the literature, although the shapes were different.

Vicker's microhardness measurements have indicated the phase hardnesses in decreasing order is most likely: Al_3Ni_2 (~800 HV_1), ϕ, (αCr) (~760 HV_1), then phases with intermediate hardness (ρ, Al_4Cr, Al_7Cr, $Al_{11}Cr_2$,

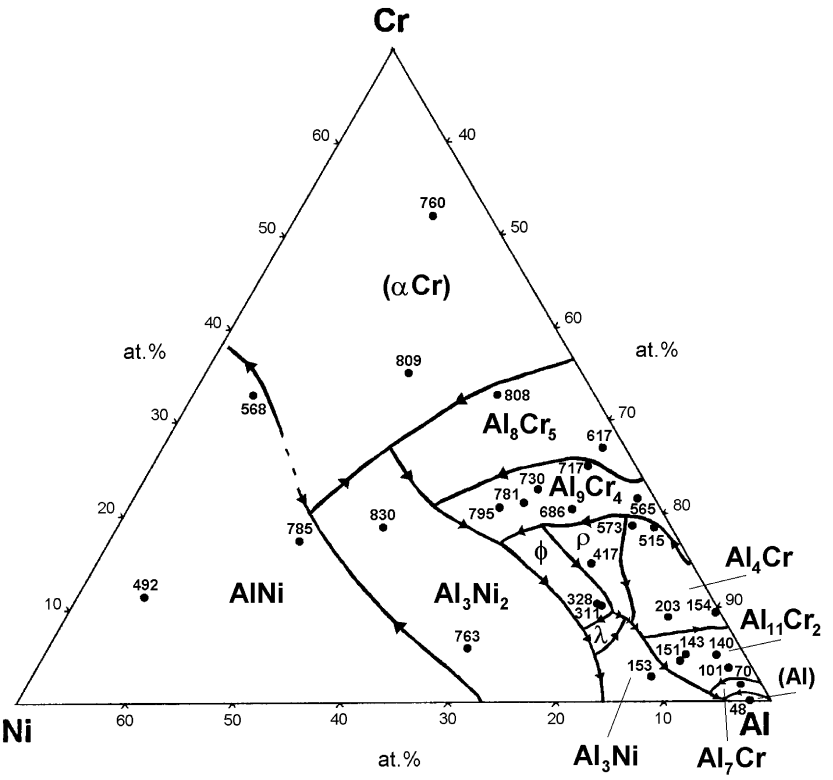

Fig. 6. Microhardness values plotted on the projection of the liquidus surface.

Al_9Cr_4), then phases with low hardness (Al_3Ni and (Al)). The ϕ, Al_4Cr, $Al_{11}Cr_2$ and Al_3Ni phases were brittle in massive form.

Acknowledgements

Mintek, D.A.C.S.T., CSIR (Mattek) and the Foundation for Research and Development are thanked for providing support. One of us (M.J.W.) thanks the University of the Witwatersrand for financial support via the Microstructural Studies Research Programme. Additionally, thanks is extended to T. Biggs for XRD measurements and Dr. I. Wolff for encouragement; both from Mintek.

References

[1] J.R. Nicholls, P. Hancock, L.H.A. Yasiri, Mater. Sci. Tech. 5 (1989) 799–812.
[2] S.R. Saunders, J.R. Nicholls, Mater. Sci. Tech. 5 (1989) 780–798.
[3] G.W. Goward, Mater. Sci. Technol. 2 (3) (1986) 194–200.
[4] B. Gleeson, W.H. Cheung, W. Da Costa, D.J. Young, Oxid. Met. 38 (1992) 407.
[5] R. Bianco, M.A. Harper, R.A. Rapp, J. Metals 43 (11) (1991) 68–73.
[6] H. Okamoto, P.R. Subramanian, L. Kacprzak (Eds.), Binary Alloy Phase Diagrams, 2nd Edition, William W. Scott Jr, OH, USA, 1990, Ed.-in-chief T.B. Massalski.
[7] S.M. Merchant, M.R. Notis, Mater. Sci. Eng. 66 (1984) 47–60.
[8] I.I. Kornilov, R.S. Mints, Ixv. Sekt. Fiz.-Khim. Anal., Inst. Obschch. Neorg. Khim., Akad. Nauk SSSR 22 (1953) 111–116, (in Russian) (from 7).
[9] D.C. Tu, Ph.D. Thesis, State University of New York at Stony Brook, 1982 (from 7).
[10] M. Audier, M. Durand-Charre, E. Laclau, H. Klein, J. Alloys Comp. 220 (1995) 225–230.
[11] E. Rosell-Laclau, M. Durand-Charre, M. Audier, J. Alloys Comp. 233 (1996) 246–263.
[12] W. Huang, Y.A. Chang, Intermetallics 7 (1999) 863–874.
[13] N. Dupin, Ph.D. Thesis, Institut National Polytechnique de Grenoble, France, 1995 (from 12).
[14] W. Huang, Y.A. Chang, Intermetallics 6 (1998) 487–498.
[15] I. Ansara, N. Dupin, H.L. Lukas, B. Sundman, J. Alloys Comp. 247 (1997) 20–30.
[16] K. Vedula, P.S. Khadkikar, in: S.H. Whang, C.T. Lui, D.P. Pope, J.O. Stieger (Eds.), High Temperature Intermetallics, The Minerals, Metals and Materials Society, 1990, pp. 197–217.
[17] R.D. Noebe, R.R. Bowman, J.T. Kim, M. Larsen, R. Gibala, in: S.H. Whang, C.T. Lui, D.P. Pope, J.O. Stieger (Eds.), High Temperature Intermetallics, The Minerals, Metals and Materials Society, 1990, pp. 271–300.
[18] I. Baker, P.R. Munroe, in: S.H. Whang, C.T. Lui, D.P. Pope, J.O. Stieger (Eds.), High Temperature Intermetallics, The Minerals, Metals and Materials Society, 1990, pp. 425–452.
[19] H.-J. Schäfer, Ph.D. Thesis, RWTH University, Aachen, Germany, 1997.
[20] J.H. Westbrook, J. Electrochem. Soc. 103 (1956) 54.
[21] D.B. Miracle, S. Russell, C.C. Law, Proc. MRS 133 (1989) 225.
[22] C.C. Law, M.J. Blackburn, Report FR-18674-4, Pratt and Whitney Group, 1985.
[23] G. Frommeyer, C. Derder, J. Phys. III France 7 (1997) 2393–2403.
[24] CC Miller program by C.L. Churms, National Accelerator Centre, P.O. Box 72, Faure, S. Africa.
[25] Crystallographica, vers. 1.60, Oxford Cryosystems, 1995–99.
[26] D.N. Compton, L.A.Cornish, M.J. Witcomb, J. Alloys Comp. (submitted).
[27] L.A. Cornish, M.J. Witcomb, P.J. Hill, I.J. Horner, S. Afr. J. Sci. 95 (1999) 517–525.
[28] I.M. Wolff, G. Sauthoff, Metall. Mater. Trans. A 27A (1996) 1395–1400.
[29] I.J. Horner, M.Sc. Dissertation, University of the Witwatersrand, Johannesburg, South Africa, 1996.